Tribological assessment of coated piston ring-cylinder liner contacts under bio-oil lubricated conditions

Peng, Yubin; Xu, Yufu; Geng, Jian; Dearn, Karl D.; Hu, Xianguo

DOI:
10.1016/j.triboint.2016.12.004
10.1016/j.triboint.2016.12.004

Document Version
Peer reviewed version

Citation for published version (Harvard):
Peng, Y, Xu, Y, Geng, J, Dearn, KD & Hu, X 2017, 'Tribological assessment of coated piston ring-cylinder liner contacts under bio-oil lubricated conditions', *Tribology International*, vol. 107, pp. 283-293. https://doi.org/10.1016/j.triboint.2016.12.004, https://doi.org/10.1016/j.triboint.2016.12.004

Tribological assessment of coated piston ring-cylinder liner contacts under bio-oil lubricated conditions

Yufu Xu[a*], Yubin Peng[a], Jian Geng[a], Karl D. Dearn[b], Xianguo Hu[a]

a. Institute of Tribology, School of Mechanical and Automotive Engineering, Hefei University of Technology, Hefei 230009, China

b. School of Mechanical Engineering, University of Birmingham, Edgbaston, Birmingham B152TT, United Kingdom

Abstract: To alleviate high friction and corrosive wear in piston ring and cylinder liner friction pairs lubricated with bio-oil, four kinds of coatings: Ni-P, Ni-P-MoS_2, Ni-P-GO (graphene oxide), and Ni-P-MoS_2-GO have been prepared via chemical nickel plating technology. An multi-functional engine cylinder liner - piston ring tribometer was employed to evaluate their tribological behaviors. Scanning electronic microscopy (SEM) was used for observing the surfaces before and after friction. Energy dispersive X-Ray spectroscopy (EDX) and X-ray photoelectron spectroscopy (XPS) were applied to measure the components and their chemical valences of the coatings surfaces before and after sliding, respectively. Furthermore, the chemical groups of the bio-oil under different frictional conditions were analyzed by Fourier transform infrared spectroscopy (FTIR). The results show that adhesive wear, stratching, spalling and mild wear took place respectively on the worn surfaces of piston rings with Ni-P, Ni-P-MoS_2, Ni-P-GO, and Ni-P-MoS_2-GO coatings. Ni-P-MoS_2-GO coated piston rings showed excellent friction-reducing and anti-wear performance and subsequently has great potential for accelerating the application of bio-oil in IC engines.

* Corresponding author. Tel.: +86 551 62901359; fax: +86 551 62901359.

E-mail: xuyufu@hfut.edu.cn

Research Highlights:

- Tribo-behaviour of Ni-P, Graphene Oxide (GO) and MoS_2 coating with bio-oil tested
- The corresponding tribological mechanisms were discussed
- Ni-P- MoS_2 coatings significantly reduce adhesive and delamination wear
- Ni-P-MoS_2-GO coatings show the lowest friction coefficient and wear
- Corrosive wear eliminated by catalytic esterification between bio-oil and Ni-P-MoS_2-GO coating

Keywords: Sliding wear; Lubricant additives; Internal combustion engines; Tribochemistry

1. Introduction

Piston ring and cylinder liner friction pairs are almost the most important parts in the internal combustion (IC) engines because more than 30% of the energy consumption in an IC engine is caused by the piston ring - cylinder liner system [1]. To cope with the energy shortage and enhance the fuel efficiency, decrease of the friction and wear of the piston ring - cylinder liner contacts has attracted lots of researchers. Etsion et al [2] used laser surface textured piston rings to improve the fuel efficiency. They found that the laser texturing did not alter the exhaust gas components, but the laser-textured piston rings could reduce the fuel consumption by 4%, comparing with those without texture. However, under corrosive conditions, surface texture might not play a protective role for piston ring - cylinder liner contacts, while coatings on friction pairs have been considered as an effective method to decrease the corrosive wear.

Skopp et al [3] analyzed the tribological behavior of titanium suboxide coatings for piston ring/cylinder liners under different conditions. It was found that thermally sprayed titanium suboxide coatings for piston ring exhibits a similar friction and wear performance to commercial

Mo-based coatings on piston ring. Cylinder liner-piston ring material with diamond like carbon (DLC) coatings exhibited better friction and wear performance than uncoated stainless [4]. Two kinds of coatings including thermal-sprayed CrN and physical vapor deposited DLC on the nitrided stainless steel and chrome plated stainless steel piston rings have been studied by Tung et al [5] under fully-formulated engine oils. Results showed that DLC coating had the lowest wear on cylinder liner. Unfortunately, DLC coating has a high internal stress [6], which leads to an abrupt spalling for coating. Chemical plating coating has become popular in recent decades, because of its lower internal stress, excellent mechanical properties, good anti-corrosion and anti-wear performances [7].

On the other hand, recently, bio-oil has become one of the most promising alternatives to fossil fuel, which has many advantages including reproducible, carbon-neutral, and environmental friendly [8]. However, high contents of acidic components makes bio-oil easy to corrode the metal, which results in it cannot be used in IC engines directly [9]. Coating is an effective method to prevent metals from corrosion of bio-oil. In our previous work, electroless Ni-P and Ni-Cu-P coating was prepared on engine cylinder liner and their tribological behavior lubricated by bio-oil has been investigated [7] . The Ni–Cu–P coating on cylinder liner has demonstrated a very potential to accelerate the application of bio-oil in IC engines. Nevertheless, to the best of our knowledge, few reports has covered the friction and wear behavior of coated piston rings lubricated by bio-oil. In this work, four kinds of coatings including Ni-P, Ni-P-MoS_2, Ni-P-GO, and Ni-P-MoS_2-GO have been deposited on piston rings and their tribological properties have been compared. Finally, the corresponding mechanisms were explored.

2. Experimental

2.1 Materials

The cylinder liner samples were made from boron cast iron and supplied by the Kaishan Cylinder Co. Ltd (China). Samples were cut to 122 mm in length, 15.6 mm in width and 6.3 mm in height. The top piston ring specimens were ductile iron and purchased from the Nanjing Feiyan Piston Ring Co., Ltd (China). The test rings were cut to 8mm in length, 2mm in width and 4mm in height. The Anhui Province Key Laboratory of Biomass & Clean Energy at the University of Science and Technology of China supplied the bio-oil used in this research, the composition and physiochemical properties can be can be found in previous work [10].

For the preparation of the coatings, nickel sulfate ($NiSO_4 \cdot 6H_2O$) was purchased from the Shanghai Liangren Chemical Co., Ltd (China). Sodium hydroxide (NaOH), sodium carbonate (Na_2CO_3), Sodium hypophosphite ($NaH_2PO_2 \cdot H_2O$) and sodium acetate (CH_3COONa) were purchased from Sinopharm Chemical Reagent Co., Ltd. Sodium citrate ($Na_3C_6H_5O_7 \cdot 2H_2O$) was supplied by the Guangdong Shantou Xilong Chemical Company. The lactic Acid ($C_3H_6O_3$), thiourea (NH_2CSNH_2) and molybdenum disulfide (MoS_2) were all received from the Shanghai Chemical Reagent Co., Ltd. Finally, the propionic acid ($C_3H_6O_2$) was purchased from the Tianjin Guangfu Fine Chemical Research Institute. All of the chemicals were of analytical grade, and used as received without further processing. The graphene oxide (GO) used in the coatings was prepared according to previous work [11].

2.2 Coating preparation

The piston ring samples were put into an alkaline solution (NaOH 50 g/L; Na_2CO_3 25 g/L) at 80 ^{o}C to degrease, and then washed by deionized water. The samples were then immersed in 50% dilute hydrochloric acid until uniform minute bubbles occurred on their surfaces, they were then

washed with deionized water. The test specimens were then placed in a plating bath solution for 60 min with a stirring speed of 300 rpm. A list of detailed process parameters is given in **Table 1**. After plating, the specimens were washed with deionized water and dried at 40 ^{o}C in a vacuum drying oven.

2.3 Coating characterization

A JEOL JSM-5600LV Scanning Electron Microscope (SEM) coupled with an Energy Dispersive X-ray spectrometer (EDX) was used to observe the micro-morphologies and detect the elemental compositions of the coating surfaces. The crystal structures of the coatings were analyzed using a Rigaku D/MAX2500V X-ray Diffraction (XRD) instrument with Cu Kα radiation, 2θ varying from 5° to 90° and a scanning velocity of $10°\cdot min^{-1}$. The micro hardness of the coatings was measured using an MH-3 micro-vickers hardness tester at a load of 0.98 N for 10 s. Each sample was tested ten times, and the hardness value of each coating was calculated from the average of these values.

2.4 Tribological tests

The friction and wear tests were carried out on a multi-functional piston ring- cylinder liner tribometer. The schematic diagram of the friction pairs are shown in **Fig. 1**. As can be seen, the piston ring slides on the cylinder liner via a reciprocating friction mode during the frictional process, with oil supplied through a drip feed. A more detailed test specification is given in **Table 2**. The coefficient of friction was recorded automatically via the ratio of friction force to normal load. The wear loss of the friction pairs was calculated by the weight of the samples before and after sliding, to an accuracy of 0.1 mg. Each test was repeated three times to obtain a standard

deviation.

After friction, the bio-oil was collected from each testing condition. The samples were washed by acetone and ultrasonically clean for 30 min. The worn surfaces of the piston ring were then observed by SEM, and the bonding energy of the typical active elements including C, O, Ni, P, Mo and S on the worn surfaces were characterized by a Thermo Scientific ESCALAB250Xi X-ray photoelectron spectroscopy (XPS) with a monochromatized Al Kα x-ray source. The chemical shifts of XPS peaks were standardized by the C 1s peak at 284.6 eV.

3. Results and discussion

3.1 Coating components and structures

Fig. 2 shows the SEM images of the four coatings, with insets showing a magnified area. The Ni–P coating displayed a relatively smooth surface with a typical cauliflower-like micro-morphology (Fig. 2a), which is similar to literature results [for example 12]. Fig. 2b shows the effect of the introduction of MoS_2, with grains and 'debris' observed on surfaces, indicating that the MoS_2 was embedded in the Ni–P matrix via the co-deposition process [13]. Some porous structures can be seen on the surfaces of Ni-P-GO coating in Fig.2c, in contrast to Wu *et al.*s observed nodular structures [14]. This may be because the graphene oxide interfered with the deposition of the Ni-P coating, as a result of the sodium dodecyl sulfate used as a surfactant for the GO during ultrasonic dispersion. This was not the case when GO and MoS_2 were used together. This produced a pristine coated surface shown in Fig.2d, with more grains and far less porosity, compared with those in Fig 2b and Fig. 2c.

Fig. 3 shows the XRD spectra of the coatings. As shown in the figure, there was a steamed-bun-like peak in each of these four coatings at 40-50 ^{o}. This was the typical amorphous

structure of Ni-P matrix [15]. It has been reported that amorphous structures are helpful to anti-friction and antiwear properties of a coating [16], therefore, heat treatment for crystallization process did not use. Furthermore, 2θ at 14.4 ^{o} were the (002) peaks of MoS_2 in Ni-P-MoS_2 and Ni-P-MoS_2-GO coatings [17, 18], which confirmed the MoS_2 was deposited in these two coatings. However, the peaks for GO did not be detected in Ni-P-GO and Ni-P-MoS_2-GO. This may because GO in the coating were total coved by Ni-P matrix and the exposed GO was easy to be removed during the preparing process, and leaving some holes on the Ni-P-GO surfaces.

Fig. 4 gives the EDX spectra of the four coating surfaces. The typical elements including Ni, P and contaminated C and O were detected in all these four coatings. Besides these elements, Mo and S were both detected in Ni-P-MoS_2 and Ni-P-MoS_2-GO coatings. These results agreed well with the former SEM and XRD results in Fig.2 and Fig.3, respectively. The contents of these elements were shown in **Table 3**. It can be found that the contaminated C was little on the Ni-P coating. However, it amounted to more than three times of contaminated C on those of Ni-P-MoS_2. This may because the rough surfaces of the Ni-P-MoS_2 coating made it more easy to be contaminated [19]. Although the content of C on Ni-P-GO coating surface was less than that of Ni-P-MoS_2 coating surface, the content of O had the opposite results, which resulted from the fact that the C and O mainly came from the GO. As for Ni-P-MoS_2-GO coatings, the contaminated and self-possessed C and O were also important on their surfaces.

Fig. 5 displays the micro-hardness of the four coating surfaces. It can be noted that adding MoS_2 had little influence on the micro-hardness of Ni-P coating, but adding GO decreased the micro-hardness of Ni-P coating obviously. This result is interesting, because GO had a high hardness [20]. It can reasonably be assumed that the few contents of GO and porous structures of the Ni-P-GO coating accounted for this result. When MoS_2 and GO used together, the hardness of

Ni-P-MoS_2-GO coatings increased a little comparing with that of Ni-P-GO coatings.

3.2 Friction and wear behaviors

Fig. 6a shows the variation of friction coefficient with time of the four different coatings. The run-in stage of these four coatings kept about 27 min, after that, all of them entered into stable friction stage [8]. Among these four coatings, Ni-P-GO coating has the highest friction coefficient, and followed by Ni-P coating, and then is Ni-P-MoS_2 coating. The Ni-P-MoS_2-GO coating has the lowest friction coefficient. This may because Ni-P-GO coating with a porous surface will destroy the formation of the lubricating oil film [21]. MoS_2 and GO might have a synesthetic effect [22] to reduce the friction of the Ni-P-MoS_2-GO coating.

Although the wear of Ni-P and Ni-P-MoS_2 coatings have very low wear loss in **Fig.6b**, the counterpart cylinder liners have high wear loss. This may because high micro-hardness of Ni-P and Ni-P-MoS_2 coatings makes the counterpart easy to be cut [23]. The cylinder liner has a low wear loss with the Ni-P-GO coating, but the Ni-P-GO coating has about 7 times wear loss than Ni-P or Ni-P-MoS_2 coating. The Ni-P-MoS_2-GO coating have a relatively low wear loss for both of the cylinder liner and piston ring. Therefore, combined use of MoS_2 and GO can improve the properties of Ni-P coating and protect the surface of friction pairs from severe friction and wear.

3.3 Tribological mechanisms

Fig. 7 shows the SEM images of worn surfaces of the piston ring with different coatings. Compared with the pristine surfaces without coating [7], there are no clear corrosive wear on these four coating surfaces, indicating these coatings could prevent the surfaces from corrosion of bio-oil under testing conditions. In addition, comparing with all the coatings before sliding, there

are obvious changes on the worn surfaces. Some delamination and adhesive phenomena occurred on the Ni-P coatings. Many dense furrows uniformly distributed on the Ni-P-MoS_2 coatings. Some pits and furrows distributed non-uniformly on the Ni-P-GO coatings. The Ni-P-MoS_2-GO had the smoothest surface with slim and few furrows. That is, introduction of MoS_2 can prevent the Ni-P coating from delamination and adhesive wear; introduction of GO alone might lead to Ni-P coating become loose and porous and easy to be removed during sliding, resulting in a higher friction coefficient and wear loss of the coating; the synergetic effects of MoS_2 and GO results in an excellent friction and wear properties of Ni-P-MoS_2-GO coatings.

To further explore what happened during sliding process, the bio-oil before and after sliding is analyzed by a Nicolet 67 Fourier-transform infrared spectrometer (FTIR, Thermo Nicolet, USA). As shown in **Fig. 8**, the peaks at 3327 cm^{-1} belong to stretching vibration of association hydroxyl group (O–H) [24], and are found in all these oils. However, the shape of this absorption band under Ni-P-GO and Ni-P-MoS_2-GO coating became narrower than the others, indicating carboxyl group (-COOH) of the bio-oil decreased [25]. The peaks at ~2946 cm^{-1} are attributed to C–H stretching [26], and comparing with bio-oil before sliding, they increase after sliding, indicating some oxygen-containing compounds have adsorbed on the rubbing surfaces. The peaks at 1709 cm^{-1} belong to carbonyl group (C=O) [27], and they are enhanced after sliding, suggesting the increase of esters contents because of the tribo-induced esterification. Besides the inner reactions of inside organic acids and alcohols, GO offers many active hydroxyl and carboxyl groups. The peak at 756 cm^{-1} is ascribed to out-of-plane bending vibration of C–H bonding [28], and it increase after sliding, which is consistent with the peaks at 2946 cm^{-1}. All these results indicate that esterification reaction occurred in the bio-oil during the sliding process, and some esters were produced.

C1s and O1s XPS spectra of worn surfaces with different coatings are shown in **Fig. 9**. As shown in the C1s spectra, the peaks at 288.7, 286.6, 284.6 and 282.9 eV are ascribed to the -COOR, C=C, C-C(C-H) groups and carbides, respectively, indicating some organics including esters, alkenes, and chemicals with hydrocarbon chain has been adsorbed or reacted on the worn surfaces [29]. These organics mainly came from the bio-oil, indicating the esterified components in bio-oil play an important lubricating role during the sliding process. The C=C group may be offered by GO in the coatings, because the peaks at 286.6 eV in Ni-P-GO and Ni-P-MoS_2-GO are much larger than those in Ni-P-MoS_2 and Ni-P coating. In addition, the peaks positioned at 282.9 belong to the carbide [30], indicating some carbons reacted with the metal elements in the coating, and formed a complex lubricating film. The O1s spectra can be resolved into two peaks. The peaks at ~529.5 eV belong to metal oxides [31]; and the peaks at 531.4 eV are ascribed to sulfates [32].

The Ni2p and P2p XPS spectra are shown in **Fig. 10**. The peaks at 853.8 eV and 871.2 eV are attributed to Ni2p3/2 and Ni2p1/2, respectively, and matched well with NiO [33]. This suggests that a NiO tribo-film is formed during the sliding process. These results agree with the O1s spectra. In P2p spectra, the lager peaks at 129.8 eV belong to the red phosphorus, and the small peaks at 133.1 eV are contributed to the pyrophosphate on the surfaces [7, 34], again confirming the tribo-reaction between the coatings and the components in bio-oil, and these findings also were in accord with our previous studies [7].

Fig. 11 shows the Mo3d and S2p XPS spectra of the worn surfaces of Ni-P-MoS_2 and Ni-P-MoS_2-GO coatings. Although there are some noises in the curves, three typical Mo3d bands can be seen, which positioned at 232.3, 229.6 and 228.5 eV, respectively. They can be attributed to MoO_3, MoS_2, and Mo_2C, respectively [35-37]. The peaks at 170.4, 167.7 and 162.3 eV in S2p

spectra are attributed to sulfates, sulfites, and MoS_2 [38, 39], which agree with the signals in O1s and Mo3d. This indicates that MoS_2 can be adsorbed or reacted on the coating surfaces to consist of a complex tribo-film.

Table 4 presents the elemental contents of the piston ring surfaces after sliding. Compared with those before sliding, the contents of carbon and oxygen increase obviously, suggesting lots of organics in bio-oil has been adsorbed or reacted on the rubbing surfaces. The contents of nickel and phosphorus decreases clearly, due to the covering by carbon and oxygen. Ni-P-GO coating has low contents of carbon, oxygen and nickel on the rubbing surfaces, which denotes a poor lubrication condition, resulting in a high friction coefficient and wear loss of the coating. Although the contents of carbon and oxygen is also low in Ni-P-MoS_2-GO coating, the contents of nickel, phosphorus , molybdenum, and sulfur are the highest, and the tribo-film composed by all these components may effectively act as a thick protective layer to prevent the surfaces from severe friction and wear. Furthermore, the relative contents of molybdenum and sulfur on Ni-P-MoS_2-GO worn surfaces even higher than those on pristine surfaces. This may because GO can remain MoS_2 on the surfaces and prevents its oxidation [22].

4. Conclusions

In this work, four kinds of coatings including Ni-P, Ni-P-MoS_2, Ni-P-GO and Ni-P-MoS_2-GO have been prepared on the piston rings. A multi-function cylinder liner – piston ring tribometer was used for measure their tribological behavior. Introduction of MoS_2 in Ni-P coating can prevent the surfaces from adhesive and delaminated wear under bio-oil lubrication conditions. Introduction of GO in Ni-P coating leads to a porous surface and increase the friction and wear. Both of MoS_2 and GO added into Ni-P coating will account for an excellent lubricating

role. Besides the tribo-film composed of components in the coatings, the adsorbed film came from the organics in the bio-oil plays an important role in antifriction and antiwear, and the Ni-P-MoS_2-GO coatings shows a great potential for preventing the corrosion of bio-oil and accelerating its application. This is because on one hand, MoS_2 and GO have synergistic lubricating effects; on the other hand, hydroxyl groups in GO can react with the carboxyl groups in bio-oil and lead to catalytic esterification reactions of bio-oil during the sliding process, which reduced the corrosive wear of bio-oil significantly.

Acknowledgments

This project is supported by the National Natural Science Foundation of China (Grant No. 51405124), China Postdoctoral Science Foundation (Grant Nos. 2015T80648, 2014M560505) and the Anhui Provincial Natural Science Foundation (Grant No. 1408085ME82).

References

[1] K. Holmberg, P. Andersson, N.-O. Nylund, K. Mäkelä, A. Erdemir, Global energy consumption due to friction in trucks and buses, Tribol. Int. 78 (2014) 94-114.

[2] I. Etsion, E. Sher, Improving fuel efficiency with laser surface textured piston rings, Tribol. Int. 42 (2009) 542-547.

[3] A. Skopp, N. Kelling, M. Woydt, L.M. Berger, Thermally sprayed titanium suboxide coatings for piston ring/cylinder liners under mixed lubrication and dry-running conditions, Wear 262 (2007) 1061-1070.

[4] H.M. Mobarak, H.H. Masjuki, E.N. Mohamad, S.M.A. Rahman, K.A.H.A. Mahmud, M.

Habibullah, S. Salauddin, Effect of DLC coating on tribological behavior of cylinder liner-piston ring material combination when lubricated with jatropha oil, Procedia Engineering 90 (2014) 733-739.

[5] S.C. Tung, H. Gao, Tribological characteristics and surface interaction between piston ring coatings and a blend of energy-conserving oils and ethanol fuels, Wear 255 (2003) 1276-1285.

[6] P. Wang, X. Wang, T. Xu, W. Liu, J. Zhang, Comparing internal stress in diamond-like carbon films with different structure, Thin Solid Films 515 (2007) 6899-6903.

[7] Y. Xu, X. Zheng, X. Hu, Y. Yin, T. Lei, Preparation of the electroless Ni–P and Ni–Cu–P coatings on engine cylinder and their tribological behaviors under bio-oil lubricated conditions, Surf. Coat. Tech. 258 (2014) 790-796.

[8] Y. Xu, Y. Peng, X. Zheng, K.D. Dearn, H. Xu, X. Hu, Synthesis and tribological studies of nanoparticle additives for pyrolysis bio-oil formulated as a diesel fuel, Energy 83 (2015) 80-88.

[9] Y.F. Xu, X.J. Zheng, Y.G. Yin, J. Huang, X.G. Hu, Comparison and analysis of the influence of test conditions on the tribological properties of emulsified bio-oil, Tribol. Lett. 55 (2014) 543-552.

[10] Q. Lu, X.-l. Yang, X.-f. Zhu, Analysis on chemical and physical properties of bio-oil pyrolyzed from rice husk, J. Anal. Appl. Pyrol. 82 (2008) 191-198.

[11] L.J. Cote, F. Kim, J. Huang, Langmuir−Blodgett assembly of graphite oxide single layers, J. Am. Chem. Soc. 131 (2009) 1043-1049.

[12] H. Ashassi-Sorkhabi, M. Es′ haghi, Corrosion resistance enhancement of electroless Ni‐P coating by incorporation of ultrasonically dispersed diamond nanoparticles, Corros. Sci. 77 (2013) 185-193.

[13] Z. Li, J. Wang, J. Lu, J. Meng, Tribological characteristics of electroless Ni–P–MoS_2

composite coatings at elevated temperatures, Appl. Surf. Sci. 264 (2013) 516-521.

[14] H. Wu, F. Liu, W. Gong, F. Ye, L. Hao, J. Jiang, S. Han, Preparation of Ni–P–GO composite coatings and its mechanical properties, Surf. Coat. Tech. 272 (2015) 25-32.

[15] S. Alirezaei, S. Monirvaghefi, A. Saatchi, M. Ürgen, K. Kazmanlı, Novel investigation on tribological properties of Ni–P–Ag–Al_2O_3 hybrid nanocomposite coatings, Tribol. Int. 62 (2013) 110-116.

[16] P. Sahoo, S.K. Das, Tribology of electroless nickel coatings–a review, Mater. Design 32 (2011) 1760-1775.

[17] K.H. Hu, X.G. Hu, Y.F. Xu, X.Z. Pan, The effect of morphology and size on the photocatalytic properties of MoS_2, React. Kine. Mech. Cat. 100 (2010) 153-163.

[18] K.H. Hu, F. Huang, X.G. Hu, Y.F. Xu, Y.Q. Zhou, Synergistic effect of nano-MoS_2 and anatase nano-TiO_2 on the lubrication properties of MoS_2/TiO_2 nano-clusters, Tribol. Lett. 43 (2011) 77-87.

[19] Z. Li, J. Wang, J. Lu, J. Meng, Tribological characteristics of electroless Ni–P–MoS_2 composite coatings at elevated temperatures, Appl. Surf. Sci. 264 (2013) 516-521.

[20] O.C. Compton, S.W. Cranford, K.W. Putz, Z. An, L.C. Brinson, M.J. Buehler, S.T. Nguyen, Tuning the mechanical properties of graphene oxide paper and its associated polymer nanocomposites by controlling cooperative intersheet hydrogen bonding, Acs Nano 6 (2012) 2008-2019.

[21] Y.F. Xu, H.Q. Yu, X.Y. Wei, Z. Cui, X.G. Hu, T. Xue, D.Y. Zhang, Friction and wear behaviors of a cylinder liner-piston ring with emulsified bio-oil as fuel, Tribol. T. 56 (2013) 359-365.

[22] Y. Xu, Y. Peng, K.D. Dearn, X. Zheng, L. Yao, X. Hu, Synergistic lubricating behaviors of

graphene and MoS 2 dispersed in esterified bio-oil for steel/steel contact, Wear 342 (2015) 297-309.

[23] C. Zishan, L. Hejun, F. Qiangang, SiC wear resistance coating with added Ni, for carbon/carbon composites, Surf. Coat. Tech.y 213 (2012) 207-215.

[24] M. Zaverkina, V. Lodygina, E.R. Badamshina, IR-spectroscopic study of hydrogen bonds in n-butanol and its mixtures with various proton acceptors, J. Appl. Spectrosc. 81 (2014) 7-14.

[25] J.W. Kim, H.W. Lee, I.-G. Lee, J.-K. Jeon, C. Ryu, S.H. Park, S.-C. Jung, Y.-K. Park, Influence of reaction conditions on bio-oil production from pyrolysis of construction waste wood, Renew. Energ. 65 (2014) 41-48.

[26] A. Talari, C. Evans, I. Holen, R. Coleman, I.U. Rehman, Raman spectroscopic analysis differentiates between breast cancer cell lines, J. Raman Spectrosc. 46 (2015) 421-427.

[27] V. Glazunov, D. Berdyshev, Anomalous appearance of ν [C (2)= C (3)] frequencies in ir spectra of 1, 4-naphthoquinone hydroxy derivatives, J. Appl. Spectrosc. 81 (2014) 553-564.

[28] L.M. Wu, D.S. Tong, C.S. Li, S.F. Ji, C.X. Lin, H.M. Yang, Z.K. Zhong, C.Y. Xu, W.H. Yu, C.H. Zhou, Insight into formation of montmorillonite-hydrochar nanocomposite under hydrothermal conditions, Appl. Clay. Sci. (2015).

[29] Y. Xu, X. Zheng, X. Hu, K.D. Dearn, H. Xu, Effect of catalytic esterification on the friction and wear performance of bio-oil, Wear 311 (2014) 93-100.

[30] M.D. Porosoff, X. Yang, J.A. Boscoboinik, J.G. Chen, Molybdenum carbide as alternative catalysts to precious metals for highly selective reduction of CO_2 to CO, Angew. Chem. 126 (2014) 6823-6827.

[31] R.J. Toh, A.Y.S. Eng, Z. Sofer, D. Sedmidubsky, M. Pumera, Ternary transition metal oxide nanoparticles with spinel structure for the oxygen reduction reaction, Chem. Electro. Chem. 2

(2015) 982–987.

[32] W. Mu, M. Li, X. Li, Z. Ma, R. Zhang, Q. Yu, K. Lv, X. Xie, J. He, H. Wei, Guanidine sulfate-assisted synthesis of hexagonal WO_3 nanoparticles with enhanced adsorption properties, Dalton. Trans. 44 (2015) 7419-7427.

[33] H.W. Park, J.H. Bang, K.N. Hui, P.K. Song, W.S. Cheong, B.S. Kang, Characteristics of NiO–AZO thin films deposited by magnetron co-sputtering in an O_2 atmosphere, Mater. Lett. 74 (2012) 30-32.

[34] H. Li, H. Li, W.-L. Dai, W. Wang, Z. Fang, J.-F. Deng, XPS studies on surface electronic characteristics of Ni–B and Ni–P amorphous alloy and its correlation to their catalytic properties, Appl. Surf. Sci. 152 (1999) 25-34.

[35] X. Li, L. Liu, A. Wang, M. Wang, Y. Wang, Y. Chen, Creation of oxygen vacancies in MoO_3/SiO_2 by thermal decomposition of pre-impregnated citric acid under N_2 and their positive role in oxidative desulfurization of dibenzothiophene, Catal. Lett. 144 (2014) 531-537.

[36] B.L. Li, H.L. Zou, L. Lu, Y. Yang, J.L. Lei, H.Q. Luo, N.B. Li, Size‐dependent optical absorption of layered mos2 and dna oligonucleotides induced dispersion behavior for label‐free detection of single‐nucleotide polymorphism, Adv. Funct. Mater. (2015).

[37] M. Liu, T. Wang, X. Zhang, X. Fan, J. Tang, Q. Xie, H. Xue, H. Guo, J. He, A facile synthesis of highly compacted, molybdenum-embedded, ordered, mesoporous, protective carbon films of graphitic structure, Corros. Sci. 87 (2014) 297-305.

[38] P. Rao, W. Yao, Z. Li, L. Kong, W. Zhang, L. Li, Highly stable $CuInS_2$@ ZnS: Al core@ shell quantum dots: the role of aluminium self-passivation, Chem. Commun. 51 (2015) 8757-8760.

[39] K.H. Hu, J. Wang, S. Schraube, Y.F. Xu, X.G. Hu, R. Stengler, Tribological properties of

MoS_2 nano-balls as filler in polyoxymethylene-based composite layer of three-layer self-lubrication bearing materials, Wear 266 (2009) 1198-1207.

Table and Figure Captions

Table 1 Composition and operating conditions for electroless coatings.

Table 2 Tribological testing conditions

Table 3 Surface chemical composition of piston ring surfaces before tribo-test .

Table 4 Surface chemical composition of piston ring surfaces after tribo-test .

Fig. 1 Schematic diagram of the friction pairs and the tribometer

Fig.2 SEM images of coating surfaces: (a) Ni-P , (b) Ni-P-MoS_2, (c) Ni-P-GO, (d) Ni-P-MoS_2-GO

Fig. 3 XRD patterns of the four coating surfaces

Fig. 4 EDX spectra of the four coating surfaces

Fig. 5 Micro-hardness of the four coating surfaces.

Fig. 6 (a) Friction coefficient, and (b)wear loss of piston ring-cylinder liner friction pairs

Fig. 7 SEM images of worn surfaces of the piston ring with different coatings: (a) Ni-P , (b) Ni-P-MoS_2, (c) Ni-P-GO, (d) Ni-P-MoS_2-GO

Fig. 8 FTIR spectra of bio-oil before and after sliding

Fig. 9 C1s and O1s XPS spectra of worn surfaces with different coatings

Fig. 10 Ni2p and P2p XPS spectra of worn surfaces with different coatings

Fig. 11 Mo3d and S2p XPS spectra of worn surfaces of Ni-P-MoS_2 and Ni-P-MoS_2-GO coatings

Table 1 Composition and operating conditions for electroless coatings.

Composition and operating conditions	Values			
	Ni-P	Ni-P-GO	Ni-P-MoS_2	Ni-P-MoS_2-GO
GO (g/L)	/	0.1	/	0.1
MoS_2 (g/L)	/	/	1	1
$NiSO_4 \cdot 6H_2O$ (g/L)	26	26	26	26
$NaH_2PO_2 \cdot H_2O$ (g/L)	30	30	30	30
$Na_3C_6H_5O_7 \cdot 2H_2O$ (g/L)	15	15	15	15
$C_3H_6O_3$ (mL/L)	17	17	17	17
CH_3COONa (g/L)	10	10	10	10
NH_2CSNH_2 (mg/L)	1	1	1	1
$C_3H_6O_2$ (mL /L)	2	2	2	2
pH	4.5±0.1	4.5±0.1	4.5±0.1	4.5±0.1
Temperature (^oC)	88±2	88±2	88±2	88±2
Time (min)	60	60	60	60

Table 2 Tribological testing conditions

Testing conditions	Values
Reciprocating frequency	5 Hz
Stroke	80 mm
Oil feed rate	50 $mL \cdot h^{-1}$
Normal load	140 N
Temperature	85 ^{o}C
Duration	60 min

Table 3 Surface chemical composition of piston ring surfaces before tribo-test .

Piston ring surfaces coating	Chemical composition (at%)					
	C	O	Ni	P	Mo	S
Ni-P	1.98	/	81.17	16.85	/	/
Ni-P-MoS_2	7.15	9.2	68.23	15.04	0.22	0.16
Ni-P-GO	6.74	17.06	62.95	13.25	/	/
Ni-P-MoS_2-GO	10.58	8.32	65.67	15.24	0.12	0.07

Table 4 Surface chemical composition of piston ring surfaces after tribo-test

Piston ring surfaces coating	Chemical composition (at%)					
	C	O	Ni	P	Mo	S
Ni-P	63.45	25.81	6.72	4.02	/	/
Ni-P-MoS_2	72.67	19.52	3.3	2.94	0.19	1.38
Ni-P-GO	67.24	22.37	5.3	5.09	/	/
Ni-P-MoS_2-GO	57.85	20.75	7.16	8.07	0.76	5.41

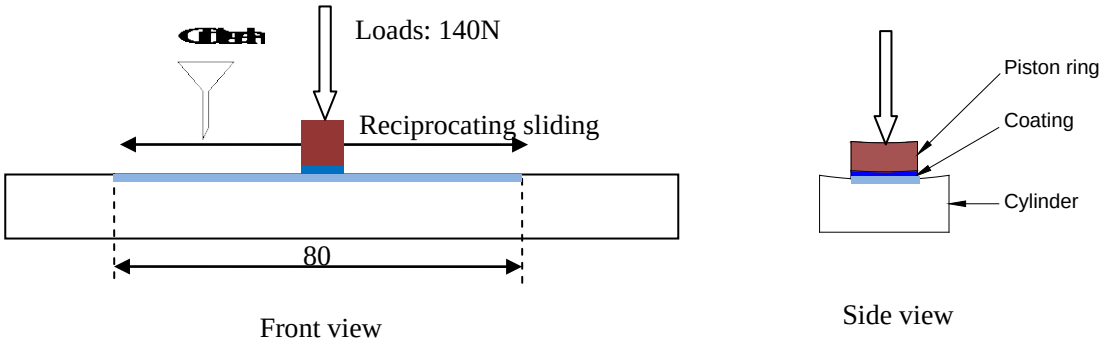

Fig. 1 Schematic diagram of the friction pairs and the tribometer

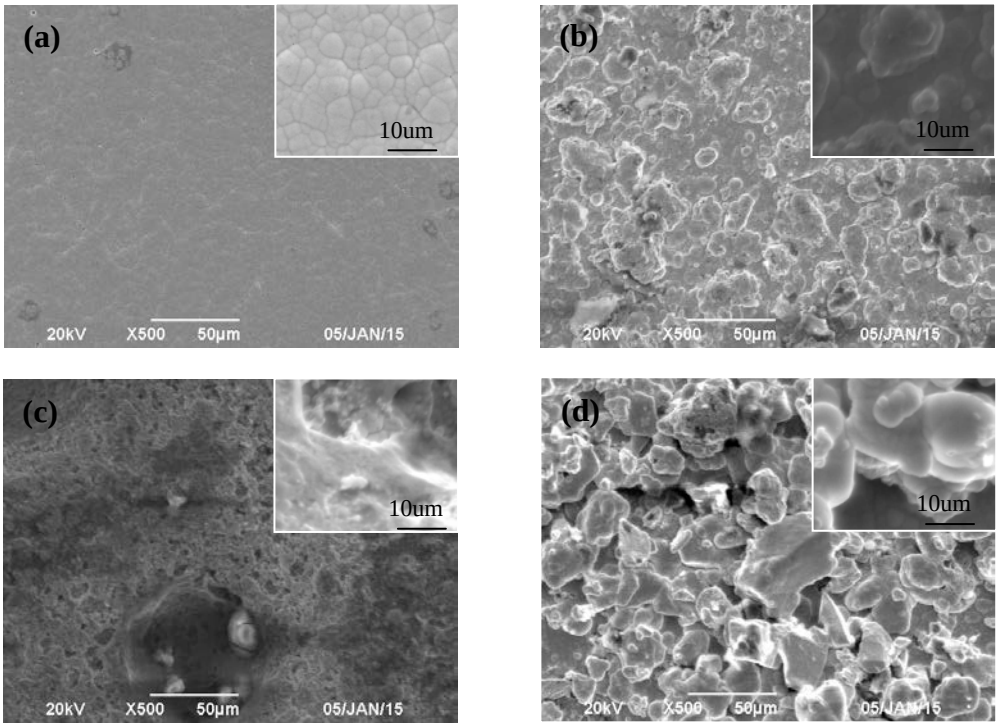

Fig.2 SEM images of coating surfaces: (a) Ni-P , (b) Ni-P-MoS_2, (c) Ni-P-GO, (d) Ni-P-MoS_2-GO

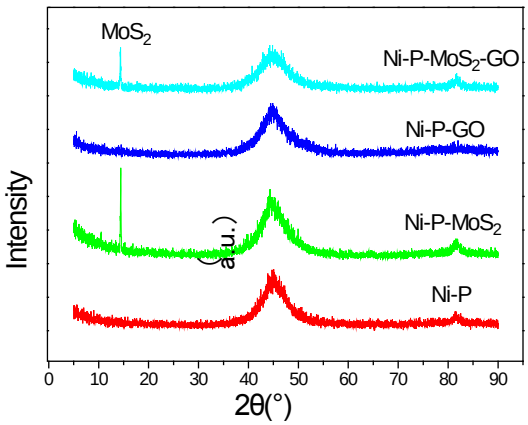

Fig. 3 XRD patterns of the four coating surfaces

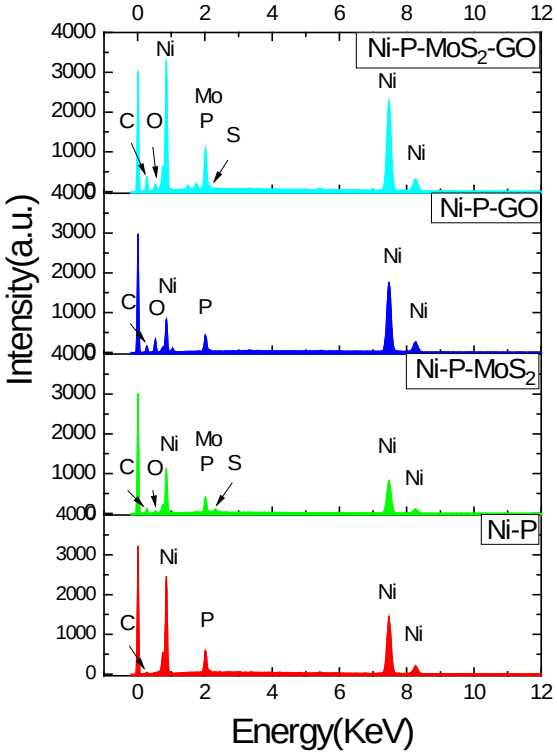

Fig. 4 EDX spectra of the four coating surfaces

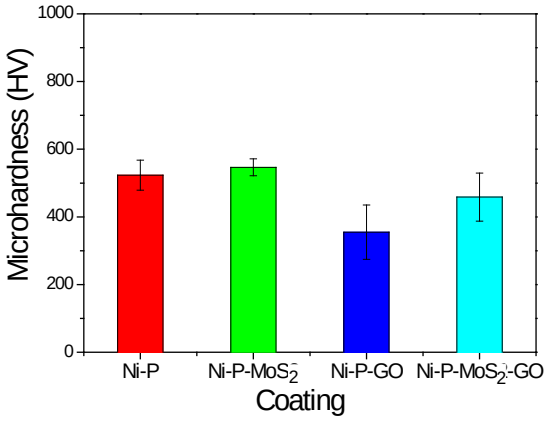

Fig. 5 Micro-hardness of the four coating surfaces

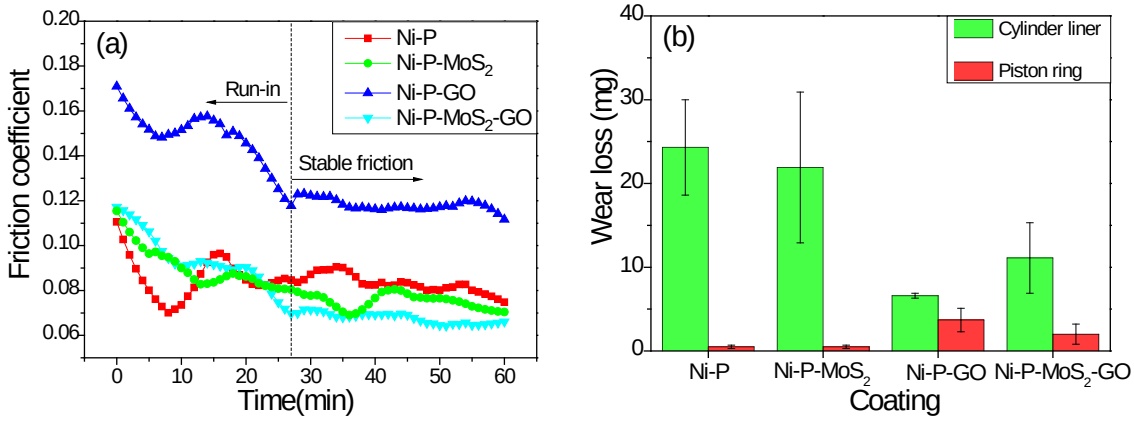

Fig. 6 (a) Friction coefficient, and (b)wear loss of piston ring-cylinder liner friction pairs

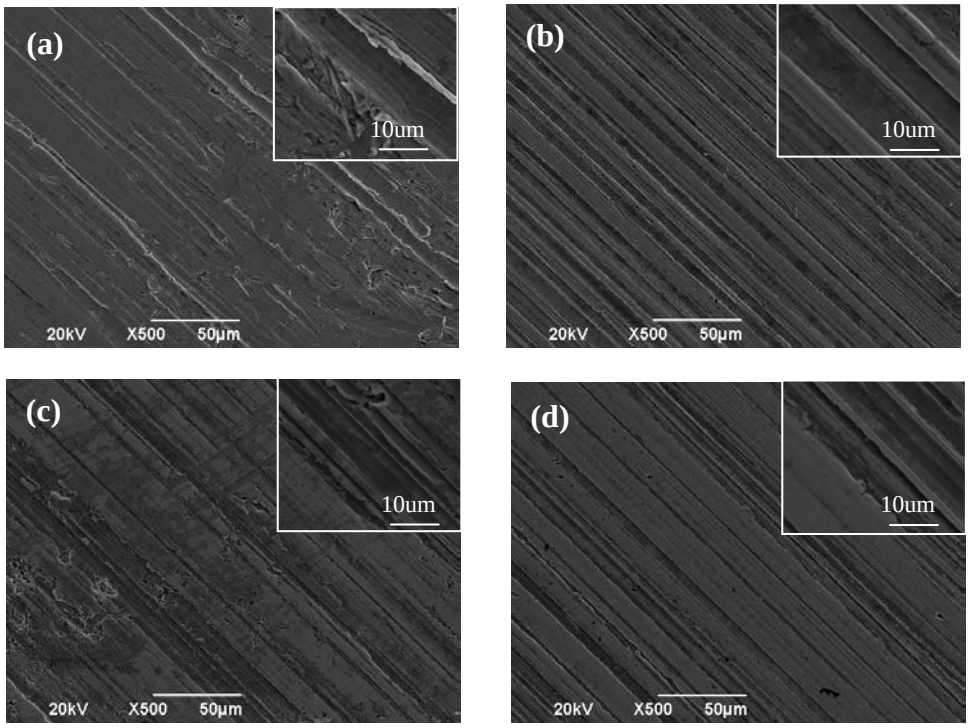

Fig. 7 SEM images of worn surfaces of the piston ring with different coatings: (a) Ni-P , (b) Ni-P-MoS_2, (c) Ni-P-GO, (d) Ni-P-MoS_2-GO

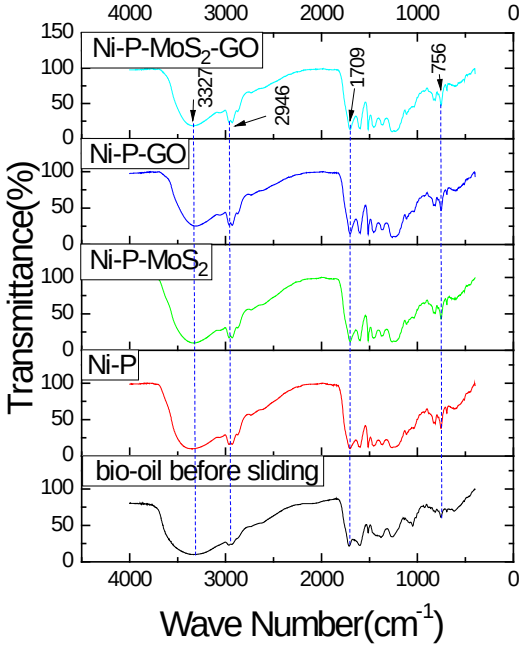

Fig. 8 FTIR spectra of bio-oil before and after sliding

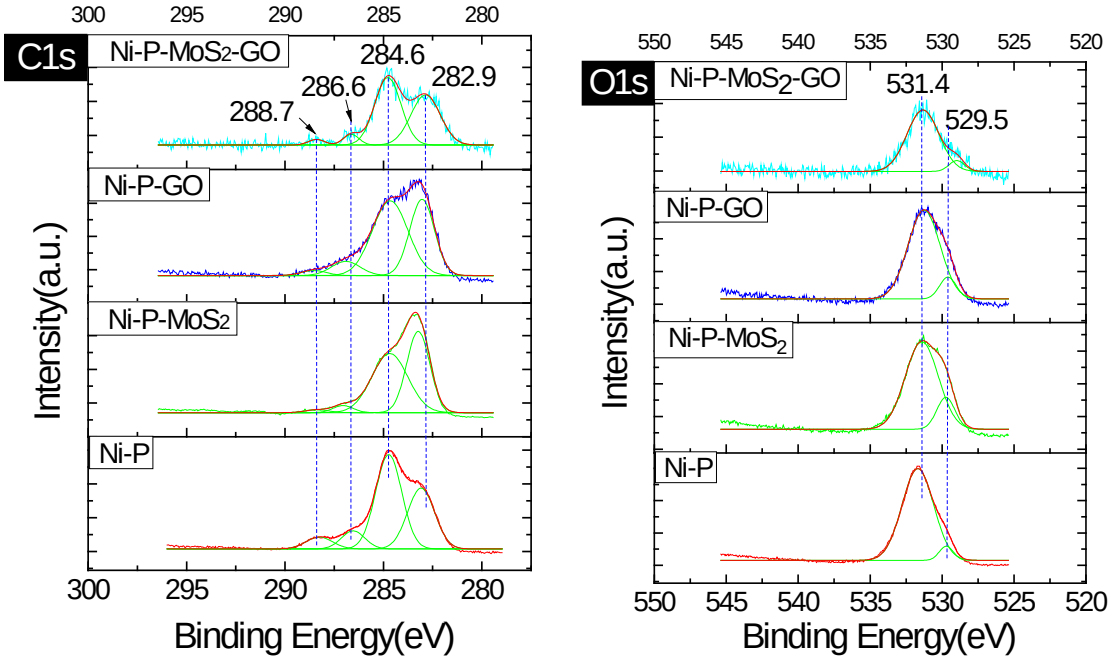

Fig. 9 C1s and O1s XPS spectra of worn surfaces with different coatings

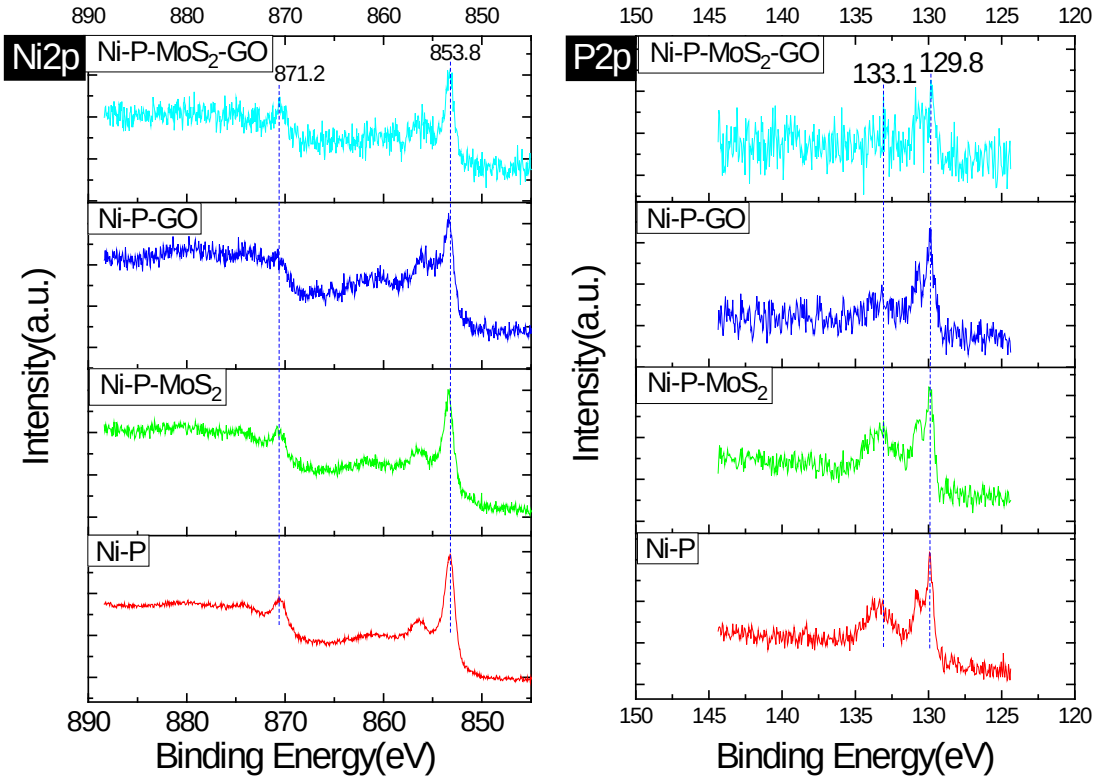

Fig. 10 Ni2p and P2p XPS spectra of worn surfaces with different coatings

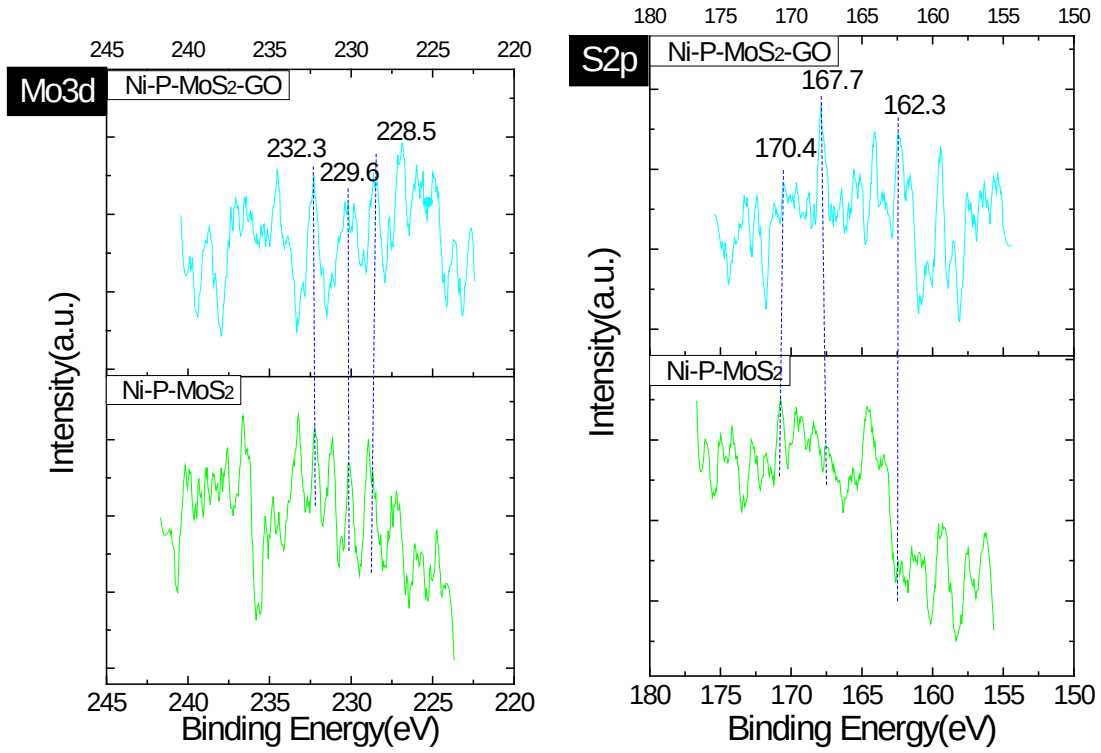

Fig. 11 Mo3d and S2p XPS spectra of worn surfaces of Ni-P-MoS_2 and Ni-P-MoS_2-GO coatings